6-2023

Shedding New Light on Weak Emission-line Quasars in the C iv-H β Parameter Space

Trung Ha
University of North Texas

Cooper Dix
University of North Texas

Brandon M. Matthews
University of North Texas

Ohad Shemmer
University of North Texas

Michael S. Brotherton
University of Wyoming

See next page for additional authors

Recommended Citation

Ha, T., Dix, C., Matthews, B. M., Shemmer, O., Brotherton, M. S., Myers, A. D., Richards, G. T., Maithil, J., Anderson, S. F., Brandt, W. N., Diamond-Stanic, A. M., Fan, X., Gallagher, S. C., Green, R., Lira, P., Luo, B., Netzer, H., Plotkin, R. M., Runnoe, J. C., ... Wu, J. (2023). Shedding New Light on Weak Emission-line Quasars in the C iv–Hβ Parameter Space. The Astrophysical Journal, 950(2), 97–.

The Astrophysical Journal, 950:97 (12pp), 2023 June 20 https://doi.org/10.3847/1538-4357/acd04d

Shedding New Light on Weak Emission-line Quasars in the C IV–Hβ Parameter Space

Trung Ha[1], Cooper Dix[1], Brandon M. Matthews[1], Ohad Shemmer[1], Michael S. Brotherton[2], Adam D. Myers[2], Gordon T. Richards[3], Jaya Maithil[4], Scott F. Anderson[5], W. N. Brandt[6,7,8], Aleksandar M. Diamond-Stanic[9], Xiaohui Fan[10], S. C. Gallagher[11], Richard Green[10], Paulina Lira[12], Bin Luo[13,14], Hagai Netzer[15], Richard M. Plotkin[16,17], Jessie C. Runnoe[18], Donald P. Schneider[6,7], Michael A. Strauss[19], Benny Trakhtenbrot[15], and Jianfeng Wu[20]

[1] Department of Physics, University of North Texas, Denton, TX 76203, USA; trungha@my.unt.edu
[2] Department of Physics and Astronomy, University of Wyoming, Laramie, WY 82071, USA
[3] Department of Physics, Drexel University, 32 S 32nd Street, Philadelphia, PA 19104, USA
[4] Center for Astrophysics | Harvard & Smithsonian, 60 Garden Street, Cambridge, MA 02138, USA
[5] Department of Astronomy, University of Washington, Box 351580, Seattle, WA 98195, USA
[6] Department of Astronomy and Astrophysics, The Pennsylvania State University, University Park, PA 16802, USA
[7] Institute for Gravitation and the Cosmos, The Pennsylvania State University, University Park, PA 16802, USA
[8] Department of Physics, 104 Davey Lab, The Pennsylvania State University, University Park, PA 16802, USA
[9] Department of Physics and Astronomy, Bates College, Lewiston, ME 04240, USA
[10] Steward Observatory, University of Arizona, 933 North Cherry Avenue, Tucson, AZ 85721, USA
[11] Department of Physics and Astronomy, University of Western Ontario, 1151 Richmond St, London, ON N6C 1T7, Canada
[12] Departamento de Astronoma, Universidad de Chile, Casilla 36D, Santiago, Chile
[13] School of Astronomy and Space Science, Nanjing University, Nanjing, Jiangsu 210093, People's Republic of China
[14] Key Laboratory of Modern Astronomy and Astrophysics (Nanjing University), Ministry of Education, Nanjing, Jiangsu 210093, People's Republic of China
[15] School of Physics and Astronomy, Tel Aviv University, Tel Aviv 69978, Israel
[16] Department of Physics, University of Nevada, Reno, NV 89557, USA
[17] Nevada Center for Astrophysics, University of Nevada, Las Vegas, NV 89154, USA
[18] Department of Physics and Astronomy, Vanderbilt University, Nashville, TN 37235, USA
[19] Department of Astrophysical Sciences, Princeton University, Princeton, NJ 08544, USA
[20] Department of Astronomy, Xiamen University, Xiamen, Fujian 361005, People's Republic of China
Received 2022 December 1; revised 2023 March 19; accepted 2023 April 9; published 2023 June 13

Abstract

Weak emission-line quasars (WLQs) are a subset of type 1 quasars that exhibit extremely weak Lyα + N V λ1240 and/or C IV λ1549 emission lines. We investigate the relationship between emission-line properties and accretion rate for a sample of 230 "ordinary" type 1 quasars and 18 WLQs at $z < 0.5$ and $1.5 < z < 3.5$ that have rest-frame ultraviolet and optical spectral measurements. We apply a correction to the Hβ-based black hole mass ($M_{\rm BH}$) estimates of these quasars using the strength of the optical Fe II emission. We confirm previous findings that WLQs' $M_{\rm BH}$ values are overestimated by up to an order of magnitude using the traditional broad-emission-line region size–luminosity relation. With this $M_{\rm BH}$ correction, we find a significant correlation between Hβ-based Eddington luminosity ratios and a combination of the rest-frame C IV equivalent width and C IV blueshift with respect to the systemic redshift. This correlation holds for both ordinary quasars and WLQs, which suggests that the two-dimensional C IV parameter space can serve as an indicator of accretion rate in all type 1 quasars across a wide range of spectral properties.

Unified Astronomy Thesaurus concepts: Quasars (1319); Active galactic nuclei (16); Supermassive black holes (1663)

Supporting material: machine-readable table

1. Introduction

Weak emission-line quasars (WLQs) are a subset of active galactic nuclei (AGNs) with extremely weak or undetectable rest-frame UV emission lines (e.g., Fan et al. 1999; Anderson et al. 2001; Collinge et al. 2005; Plotkin et al. 2010). The Sloan Digital Sky Survey (SDSS; York et al. 2000) has discovered $\approx 10^3$ type 1 quasars with Lyα + N V λ1240 rest-frame equivalent width (EW) <15.4 Å and/or C IV λ1549 EW < 10.0 Å (e.g., Diamond-Stanic et al. 2009; Meusinger & Balafkan 2014). These numbers represent a highly significant concentration of quasars at $\gtrsim 3\sigma$ deviation from the log-normal EW distribution of the SDSS quasar population, with no corresponding "tail" at the opposite end of the distribution (Diamond-Stanic et al. 2009; Wu et al. 2012). Furthermore, the fraction of WLQs among the broader quasar population increases sharply at higher redshifts (and thus higher luminosities), from $\sim$0.1% at $3 \lesssim z \lesssim 5$ to $\sim$10%–15% at $z \gtrsim 5.7$ (Diamond-Stanic et al. 2009; Bañados et al. 2016; Shen et al. 2019).

Multiwavelength observations of sources of this class have shown that they are unlikely to be high-redshift galaxies with apparent quasar-like luminosity due to gravitational-lensing amplification, dust-obscured quasars, or broad absorption line (BAL) quasars (e.g., Shemmer et al. 2006, 2010) but that their UV emission lines are intrinsically weak. Furthermore, WLQs are typically radio quiet and have X-ray and mid-infrared properties inconsistent with those of BL Lac objects

(Shemmer et al. 2009; Lane et al. 2011; Wu et al. 2012; Massaro et al. 2017).

About half of WLQs have notably lower X-ray luminosities than expected from their monochromatic luminosities at 2500 Å (e.g., Luo et al. 2015; Ni et al. 2018, 2022; Timlin et al. 2020). One explanation for this phenomenon is that, at small radii, the geometrically thick accretion disks of these WLQs are "puffed up" and prevent highly ionizing photons from reaching the broad emission-line region (BELR; e.g., Wu et al. 2011, 2012; Luo et al. 2015; Ni et al. 2018, 2022). The X-ray radiation is partially absorbed by the thick disk, resulting in low apparent X-ray luminosities at high inclinations (i.e., when these objects are viewed edge on). When these objects are viewed at much lower inclinations, their notably steep X-ray spectra indicate accretion at a high Eddington luminosity ratio ($L_{\rm bol}/L_{\rm Edd}$, hereafter $L/L_{\rm Edd}$; e.g., Shemmer et al. 2008; Luo et al. 2015; Marlar et al. 2018).

The indications of high Eddington ratios in WLQs may provide a natural explanation for the weakness of their emission lines in the context of the Baldwin effect. In its classical form, this effect is an anticorrelation between the EW(C IV) and the quasar luminosity (Baldwin 1977). Subsequent studies, however, have found that this relation stems from a more fundamental anticorrelation between EW(C IV) and Hβ-based $L/L_{\rm Edd}$ (Baskin & Laor 2004, hereafter BL04; Dong et al. 2009). This anticorrelation, coined the modified Baldwin effect (MBE), was extensively studied and built upon by Shemmer & Lieber (2015, hereafter SL15; however, see also Wang et al. 2022). SL15 utilized a sample of nine WLQs and 99 non-radio-loud, non-BAL ("ordinary") quasars spanning wide ranges of luminosity and redshift to analyze the relative strength of the C IV emission line and the Hβ-based Eddington ratio. They confirmed the findings of BL04 for the sample of ordinary quasars. However, all nine WLQs were found to possess relatively low $L/L_{\rm Edd}$ values, while the MBE predicts considerably higher Eddington ratios for these sources. This finding led SL15 to conclude that the Hβ-based $L/L_{\rm Edd}$ parameter cannot depend solely on EW(C IV) for all quasars. Such a conclusion may also be consistent with subsequent findings that WLQs possess strong Fe II emission and large velocity offsets of the C IV emission-line peak with respect to the systemic redshift (hereafter, Blueshift(C IV); Martínez-Aldama et al. 2018) and that $L/L_{\rm Edd}$ correlates with Blueshift(C IV) at high Blueshift(C IV) values (see Figure 14 of Rankine et al. 2020).

In this work, we explore two possible explanations for the findings of SL15. The first of these is that the traditional estimation of Hβ-based black hole mass ($M_{\rm BH}$) values, and therefore $L/L_{\rm Edd}$ values, fails to accurately predict $M_{\rm BH}$, particularly in quasars with strong optical Fe II emission (e.g., Shen 2013; Maithil et al. 2022). Such a case is typical for WLQs, and thus a correction via measurement of the strength of the Fe II emission complex in the optical band is required (Du & Wang 2019; Yu et al. 2020b). The second explanation is that EW(C IV), by itself, is not an ideal indicator of the quasar accretion rate. In addition to EW(C IV), we utilize a recently defined parameter, the "C IV ||Distance" (Rivera et al. 2022, hereafter R22), which represents a combination of the EW(C IV) and Blueshift(C IV) (Richards et al. 2011; Rivera et al. 2020; McCaffrey & Richards 2021), and search for a correlation between that parameter and $L/L_{\rm Edd}$.

To investigate these explanations, we extend the WLQ sample of SL15 to nine additional sources available from the Gemini Near-IR Spectrograph–Distant Quasar Survey (GNIRS-DQS; Matthews et al. 2023, hereafter Paper I). Furthermore, we study the distribution of WLQs in the $L/L_{\rm Edd}$ space versus a sample of ordinary quasars from SL15 and Paper I. We aim to investigate the underlying driver for the weak emission lines in WLQs and test the assertion that all WLQs have extremely high accretion rates.

The structure of this paper is as follows. In Section 2, we discuss our sample selection and the relevant equations used to estimate Hβ-based $L/L_{\rm Edd}$ values. In Section 3, we analyze the samples' spectroscopic properties as well as the sources' black hole masses and accretion rates. Subsequently, we discuss the correlation between the C IV parameter space and $L/L_{\rm Edd}$. In Section 4, we summarize our findings. Throughout this paper, we compute luminosity distances using a standard ΛCDM cosmology with $H_0 = 70$ km s^{-1} Mpc^{-1}, $\Omega_{\rm M} = 0.3$, and $\Omega_\Lambda = 0.7$ (e.g., Spergel et al. 2007).

2. Sample Selection and Data Analysis

2.1. WLQ Sample

We compile a sample of 18 WLQs that have accurate full-width-at-half-maximum intensity of the broad component of the Hβ λ4861 emission line (hereafter, FWHM(Hβ)), monochromatic luminosity at rest-frame 5100 Å (hereafter, νL_ν(5100 Å)), EW(Fe II $\lambda\lambda$4434–4684), and EW(Hβ) measurements. Nine of these sources were obtained from SL15, seven from the GNIRS-DQS sample of Paper I (see Section 2.2), and two from this work (see the Appendix). SL15 compiled a sample of nine WLQs: SDSS J0836+1425, SDSS J1411+1402, SDSS J1417+0733, SDSS J1447−0203 (Plotkin et al. 2010, 2015), SDSS J0945+1009 (Hryniewicz et al. 2010; Plotkin et al. 2015), SDSS J1141+0219, SDSS J1237+6301 (Diamond-Stanic et al. 2009; Shemmer et al. 2010), SDSS J1521+5202 (Just et al. 2007; Wu et al. 2011), and PHL 1811 (Leighly et al. 2007).

Table 1 provides basic properties for the 18 WLQs in our sample. Column (1) provides the source name; Column (2) gives the systemic redshift determined from the peak of, in order of preference, the [O III] λ5007, Mg II λ2798, and Hβ emission lines; Column (3) gives log νL_ν (5100 Å); Column (4) gives FWHM (Hβ); Column (5) gives $R_{\rm Fe\,II} \approx$ EW(Fe II)/EW(Hβ); Column (6) gives traditional Hβ-based $M_{\rm BH}$ estimates (following Equations (2) and (4)); Column (7) gives Fe II-corrected Hβ-based $M_{\rm BH,corr}$ estimates (following Equations (3) and (4)); Column (8) gives traditional Hβ-based $L/L_{\rm Edd}$ values (from Equation (5)); Column (9) gives Fe II-corrected Hβ-based $L/L_{\rm Edd,corr}$ values (from Equation (5)); Column (10) gives EW(C IV); Column (11) gives Blueshift(C IV); Columns (12) and (13) provide the references for the rest-frame optical and UV spectral measurements, respectively. All derived properties are discussed in detail in Section 2.4.

The two WLQs from Shemmer et al. (2010) and the two introduced in the Appendix do not have a reliable C IV line measurement in the literature; hence we perform our own measurements from their SDSS spectra, following the procedure in Dix et al. (2023, hereafter Paper II). Briefly, we fit the C IV emission line with a local, linear continuum and two independent Gaussians. These Gaussians are constrained such that the flux densities lie between 0 and twice the value of the

Table 1
Basic Properties of the WLQ Sample

Quasar	$z_{\rm sys}$	$\log \nu L_\nu$(5100 Å) (erg s^{-1})	FWHM(Hβ) (km s^{-1})	$R_{\rm Fe\ II}$	$\log M_{\rm BH}$ ($M_\odot$)	$\log M_{\rm BH,corr}$ ($M_\odot$)	$L/L_{\rm Edd}$	$L/L_{\rm Edd,corr}$	EW(C IV) (Å)	Blueshift(C IV) (km s^{-1})	Optical References[a]	C IV References[a]
(1)	(2)	(3)	(4)	(5)	(6)	(7)	(8)	(9)	(10)	(11)	(12)	(13)
SDSS J010643.23−031536.4	2.248	46.51	6782	0.58	9.99	9.71	0.20	0.39	$7.6^{+0.6}_{-0.9}$	1451^{+119}_{-60}	1	2
SDSS J013136.44+130331.0	1.599	46.45	2294	0.78	9.02	8.67	1.63	3.67	$2.8^{+1.4}_{-2.0}$	2320^{+819}_{-521}	1	2
SDSS J013417.81−005036.2	2.270	46.45	5211	0.98	9.73	9.31	0.32	0.84	$7.3^{+0.7}_{-1.0}$	2233^{+651}_{-414}	1	2
SDSS J075115.43+505439.1	2.311	46.59	3077	3.05	9.35	8.19	1.05	15.04	$6.6^{+0.6}_{-1.0}$	5953^{+234}_{-117}	1	2
SDSS J083650.86+142539.0	1.749	45.93	2880	2.48	8.94	8.04	0.62	4.95	$4.2^{+0.3}_{-0.5}$	2266 ± 191	3	3
SDSS J085337.36+121800.3	2.197	46.56	4502	0.28	9.66	9.48	0.47	0.73	$7.7^{+1.1}_{-1.7}$	1166^{+363}_{-242}	1	2
SDSS J085344.17+354104.5	2.183	46.40	4168	0.72	9.51	9.18	0.47	1.00	$4.3^{+0.8}_{-1.2}$	2053^{+1580}_{-1094}	1	2
SDSS J094533.98+100950.1	1.683	46.17	4278	2.00	9.41	8.66	0.35	2.03	$2.9^{+0.3}_{-0.6}$	5485 ± 380	3	3
SDSS J094602.31+274407.0	2.488	46.75	3833	1.65	9.63	8.94	0.79	3.82	$5.9^{+0.4}_{-0.6}$	9062^{+16}_{-11}	1	2
SDSS J113747.64+391941.5	2.428	45.81	2518	3.31	8.76	7.57	0.72	10.99	8^{+6}_{-9}	3089^{+2050}_{-1236}	4	4
SDSS J114153.33+021924.4	3.550	46.55	5900	3.25	9.89	8.67	0.27	4.60	0.4^{+2}_{-4}	-577^{+2461}_{-1484}	5	6,4
SDSS J123743.07+630144.7	3.490	46.35	5200	2.86	9.68	8.61	0.29	3.39	1 ± 2	-970^{+1349}_{-845}	5	4
SDSS J141141.96+140233.9	1.754	45.64	3966	1.41	9.06	8.56	0.24	0.78	$3.8^{+0.8}_{-0.2}$	3142^{+370}_{-208}	1	2
SDSS J141730.92+073320.7	1.716	45.91	2784	1.65	8.90	8.29	0.65	2.64	$2.5^{+2.1}_{-0.7}$	5321^{+4178}_{-872}	1	2
SDSS J144741.76 020339.1	1.430	45.56	1923	1.60	8.39	7.83	0.96	3.52	$7.7^{+0.2}_{-1.3}$	1319^{+759}_{-381}	1	2
SDSS J152156.48+520238.5	2.190	47.14	5750	1.64	10.19	9.48	0.52	2.69	9.1 ± 0.6	4900 ± 300[b]	7	7
SDSS J213742.25−003912.7	2.294	45.75	2630	2.45	8.77	7.89	0.62	4.68	3^{+1}_{-2}	4986^{+867}_{-535}	4	4
PHL 1811	0.192	45.56	1943	1.29[c]	8.40	7.94	0.94	2.70	6.6	1400 ± 250	8	8

Notes.
[a] Sources of rest-frame optical–UV data, Column (12): $z_{\rm sys}$, νL_ν(5100 Å), FWHM(Hβ), $R_{\rm Fe\ II}$; Column (13): EW(C IV), and Blueshift(C IV). (1) Paper I, (2) Paper II, (3) Plotkin et al. (2015), (4) this work, (5) Shemmer et al. (2010), (6) Shen et al. (2011), (7) Wu et al. (2011), (8) Leighly et al. (2007).
[b] Wu et al. (2011) also reported Hβ-based Blueshift(C IV) = 9400 km s^{-1}. Here, we have opted to use a Mg II-based value of Blueshift(C IV).
[c] Leighly et al. (2007) reported the $R_{\rm Fe\ II}$ value as being in the range 1.22−1.35. We have adopted a mean value of 1.29 for this work.

peak of the emission line; the FWHM is restricted to not exceed 15,000 km s^{-1}. Furthermore, we visually inspect the initial fit to correct for any additional residuals. The EW of the line emission can then be measured, as well as the blueshift, which is calculated from the difference between λ1549 and the rest-frame wavelength of the peak of the emission-line profile (see Equation (1)).

Our WLQs appear to possess stronger relative optical Fe II emission (indicated by the larger $R_{\rm Fe\,II}$ values) compared to ordinary quasars from their respective samples. Since such sources are selected based only on their C IV emission-line strength (EW(C IV) <10 Å), we are unable to assess any potential biases introduced by the rest-frame optical emission to their selection process.

2.2. Ordinary Quasar Sample Selection

In order to create a comprehensive comparison sample of quasars for our analysis, which requires measurements of both the Hβ and C IV emission lines, we select two catalogs of ordinary quasars from the literature. For the high-redshift quasars ($1.5 \lesssim z \lesssim 3.5$), C IV emission properties can be obtained from SDSS, but the Hβ emission line lies outside of the SDSS range, and therefore it has to be measured with NIR spectroscopy. In this redshift range, we utilize the GNIRS-DQS catalog in Paper I. GNIRS-DQS is the largest and most comprehensive inventory of rest-frame optical properties for luminous quasars, notably the Hβ, [O III], and Fe II emission lines. To complement this sample of high-redshift, high-luminosity quasars, we include an archival sample of quasars in the low-redshift regime from the BL04 subsample also utilized in SL15. In this redshift range ($z < 0.5$), the Hβ emission properties can be obtained from optical spectra, but the C IV emission-line properties are more difficult to obtain and are available primarily from the Hubble Space Telescope (HST) and the International Ultraviolet Explorer (IUE) archives. Below, we briefly discuss the selection process for our ordinary quasar sample.

The GNIRS-DQS sources were selected to lie in three narrow redshift intervals, $1.55 \lesssim z \lesssim 1.65$, $2.10 \lesssim z \lesssim 2.40$, and $3.20 \lesssim z \lesssim 3.50$ to center the Hβ+[O III] spectral complex in the NIR bands covered by GNIRS (i.e., the J, H, and K bands, respectively). In total, the survey comprises 260 sources with high-quality NIR spectra and comprehensive Hβ, [O III], and Fe II spectral measurements (see Matthews et al. 2021 and Paper I for more details). We exclude 64 BAL quasars, 16 radio-loud quasars (RLQs), and one quasar, SDSS J114705.24+083900.6, that is both BAL and radio loud. We define RLQs as sources having radio-loudness values of $R > 100$ (where R is the ratio between the flux densities at 5 GHz and 4400 Å; Kellermann et al. 1989). RLQs and BAL quasars are excluded to minimize the potential effects of continuum boosting from a jet (e.g., Meusinger & Balafkan 2014) and absorption biases (e.g., see BL04), respectively. Two quasars, SDSS J073132.18+461347.0 and SDSS J141617.38+264906.1, are excluded due to a lack of C IV measurements from Paper II. In total, 177 GNIRS-DQS quasars are included in our analysis; of these, seven sources with EW(C IV) <10 Å can be formally classified as WLQs (see Section 2.1). We adopt values of FWHM(Hβ), νL_ν(5100 Å), EW(Hβ), and EW(Fe II) values from Paper I. The latter two parameters are used to derive $R_{\rm Fe\,II}$. Paper II reports the EW(C IV) values and the wavelengths of the C IV emission-line peaks for the quasars in Paper I, which are then used to derive the Blueshift(C IV) values (see Section 2.3).

Sixty quasars at $z < 0.5$ from BL04 are added to our analysis from the 63 BL04 quasars in SL15. PG 0049+171, PG 1427+480, and PG 1415+451 are excluded due to a lack of published Fe II spectral measurements. The UV data in the BL04 sample comes, roughly equally, from both the HST and the IUE archives (see Baskin & Laor 2005). Throughout this work, we check whether including only HST or IUE data changes the conclusion of the paper, but we find no statistical difference in the results of Section 3. Therefore, we include both subsets in this work. We obtain the FWHM(Hβ), νL_ν(5100 Å), and $R_{\rm Fe\,II}$ values for the BL04 sources from Boroson & Green (1992) and their EW(C IV) and Blueshift (C IV) values from Baskin & Laor (2005). The line measurements are expected to be roughly consistent across the different samples utilized in this work since they all employed similar standard fitting procedures. Table 2 lists the basic properties of the ordinary quasars in our sample with the same formatting as Table 1.

2.3. Systemic Redshifts and Blueshift(C IV)

We derive the Blueshift(C IV) values of GNIRS-DQS sources from the observed wavelengths of the C IV emission-line peaks reported in Paper II and the systemic redshifts reported in Paper I. The Blueshift(C IV) values are derived following Equation (2) in Dix et al. (2020)

$$\frac{\Delta v}{\mathrm{km\ s^{-1}}} = \left[\frac{c}{\mathrm{km\ s^{-1}}}\right]\left(\frac{z_{\rm meas} - z_{\rm sys}}{1 + z_{\rm sys}}\right), \tag{1}$$

where $z_{\rm meas}$ is the redshift measured from the wavelength of the C IV emission-line peak and $z_{\rm sys}$ is the systemic redshift with respect to the [O III], the Mg II, or the Hβ emission lines reported in Paper I. In this work, we report the Blueshift(C IV) $\equiv -\Delta v$ values.

A nonnegligible fraction ($\sim$1/3) of luminous quasars have extremely weak or undetectable [O III] emission (e.g., Netzer et al. 2004), so we must use alternative emission lines as the reference for $z_{\rm sys}$ (as was done for many ordinary GNIRS-DQS sources; see Paper I). In spite of the larger intrinsic uncertainties associated with using the Mg II and Hβ emission lines as $z_{\rm sys}$ indicators ($\sim$200 km s^{-1} and $\sim$400 km s^{-1}, respectively; Shen et al. 2016), these uncertainties are typically much smaller than the Blueshift(C IV) values observed in the majority of luminous high-redshift quasars (see Paper I). Therefore, the lack of [O III]-based $z_{\rm sys}$ values for such sources should not affect the conclusions of this work significantly.

2.4. M_{BH} and L/L_{Edd} Estimates

Traditional estimation of single-epoch $M_{\rm BH}$ values has made use of the reverberation-mapping (RM) scaling relationship between the size of the Hβ-emitting region ($R_{\rm H\beta}$) and νL_ν(5100 Å) (e.g., Laor 1998; Wandel et al. 1999; Kaspi et al. 2005; Bentz et al. 2013). In this work, we use the empirical scaling relation established by Bentz et al. (2013) for consistency with other recent studies (e.g., Maithil et al. 2022; Paper II):

$$\log\left[\frac{R_{\rm H\beta}}{\mathrm{lt-days}}\right] = (1.527 \pm 0.031) + (0.533 \pm 0.035)\log \ell_{44}, \tag{2}$$

Table 2
Basic Properties of the Ordinary Quasar Sample

Quasar (1)	$z_{\rm sys}$ (2)	$\log \nu L_\nu$(5100 Å) (erg s^{-1}) (3)	FWHM(Hβ) (km s^{-1}) (4)	$R_{\rm Fe\ II}$ (5)	$\log M_{\rm BH}$ ($M_\odot$) (6)	$\log M_{\rm BH,corr}$ ($M_\odot$) (7)	$L/L_{\rm Edd}$ (8)	$L/L_{\rm Edd,corr}$ (9)	EW(C IV) (Å) (10)	Blueshift(C IV) (km s^{-1}) (11)	Optical Reference[a] (12)	C IV Reference[a] (13)
PG 0003+199	0.026	44.07	1640	0.62	7.46	7.36	0.33	0.41	60.1[b]	−102	3	4
SDSS J001018.88+280932.5	1.613	46.27	3189	0.06	9.21	9.13	0.70	0.86	$61.0^{+0.5}_{-0.8}$	203^{+22}_{-15}	1	2
SDSS J001453.20+091217.6	2.335	46.36	6428	0.72	9.87	9.54	0.19	0.40	$39.0^{+3.3}_{-5.0}$	825^{+397}_{-266}	1	2
SDSS J001813.30+361058.6	2.333	46.46	4896	0.55	9.68	9.41	0.36	0.68	$25.8^{+1.1}_{-1.6}$	2689^{+203}_{-136}	1	2
SDSS J001914.46+155555.9	2.267	46.34	4033	0.17	9.45	9.32	0.47	0.64	$44.5^{+0.9}_{-1.3}$	372^{+110}_{-74}	1	2
PG 0026+129	0.145	45.13	1860	0.51	8.13	7.98	0.68	0.95	19.3	−120	3	4
SDSS J002634.46+274015.5	2.247	46.38	4420	0.00	9.55	9.48	0.41	0.49	$134.6^{+10.1}_{-15.0}$	400^{+416}_{-279}	1	2
SDSS J003001.11-015743.5	1.590	46.10	4028	0.26	9.32	9.18	0.37	0.52	$52.7^{+1.9}_{-2.8}$	1279^{+139}_{-93}	1	2
SDSS J003416.61+002241.1	1.631	46.24	5527	0.44	9.67	9.46	0.23	0.38	$28.5^{+0.3}_{-0.5}$	597^{+86}_{-58}	1	2
SDSS J003853.15+333044.3	2.373	46.39	4297	0.50	9.53	9.28	0.44	0.78	$13.8^{+1.0}_{-1.5}$	670^{+947}_{-635}	1	2

Notes.
Only the first ten lines are shown.
[a] Source of rest-frame optical–UV data, Column (12): $z_{\rm sys}$, νL_ν(5100 Å), FWHM(Hβ), $R_{\rm Fe\ II}$; Column (13): EW(C IV), and Blueshift(C IV). (1) Paper I, (2) Paper II, (3) Boroson & Green (1992), (4) Baskin & Laor (2005).
[b] There are no errors reported for EW(C IV) and Blueshift(C IV) values for PG quasars in Baskin & Laor (2005).

(This table is available in its entirety in machine-readable form.)

where $\ell_{44} \equiv \nu L_\nu(5100\ \text{Å})/10^{44}\ \text{erg s}^{-1}$.

However, the Hβ RM sample was subsequently determined to be biased toward objects with strong, narrow [O III] emission lines and, in effect, is biased in favor of low-accretion-rate broad-line AGNs (see, e.g., Robinson 1994; Shen & Ho 2014). Recent RM campaigns aimed at minimizing such bias, such as the super-Eddington accreting massive black hole (SEAMBH; Du et al. 2014 Du et al. 2014, 2016, 2018) and the SDSS-RM project (Shen et al. 2015), found deviations from the traditional size–luminosity relationship. In particular, SEAMBHs found a population of rapidly accreting AGNs with a BELR size up to 3–8 times smaller than predicted by Equation (2), which implies an overestimation of super-Eddington-accreting $M_{\rm BH}$ values from single-epoch spectra by the same factor. We apply a $R_{\rm Fe\,II}$ correction to the traditional Hβ-based $M_{\rm BH}$ estimation, a method developed by Du & Wang (2019). The $R_{\rm Fe\,II}$ parameter has been shown to correlate with $L/L_{\rm Edd}$ (e.g., Netzer & Trakhtenbrot 2007).

For the Fe II-corrected values of $M_{\rm BH}$ (hereafter, $M_{\rm BH,corr}$), we apply the size–luminosity scaling relation for $R_{\rm H\beta}$ following Equation (5) of Du & Wang (2019):

$$\log\left[\frac{R_{\rm H\beta,\,corr}}{\rm lt{-}days}\right] = (1.65 \pm 0.06) + (0.45 \pm 0.03)\log \ell_{44} + (-0.35 \pm 0.08)\, R_{\rm Fe\,II}. \quad (3)$$

Subsequently, $M_{\rm BH}$ ($M_{\rm BH,corr}$) can be estimated using the following relationship:

$$\frac{M_{\rm BH}\ (M_{\rm BH,\,corr})}{M_\odot} = f\left[\frac{R_{\rm BELR}}{\rm pc}\right]\left[\frac{\Delta V}{\rm km\ s^{-1}}\right]^2\left[\frac{G}{{\rm pc}M_\odot^{-1}\ ({\rm km\ s^{-1}})^2}\right]^{-1} \approx 1.5\left[\frac{R_{\rm H\beta}\ (R_{\rm H\beta,\,corr})}{\rm pc}\right]\left[\frac{\rm FWHM(H\beta)}{\rm km\ s^{-1}}\right]^2 \cdot \left[\frac{4.3\times10^{-3}}{{\rm pc}M_\odot^{-1}\ (km\ s^{-1})^2}\right]^{-1}, \quad (4)$$

where we adopt $f = 1.5$ for the virial coefficient, consistent with results from Ho & Kim (2014), Yu et al. (2019, 2020a), and Maithil et al. (2022); $R_{\rm BELR} \approx R_{\rm H\beta}$ ($R_{\rm H\beta,\,corr}$) is the size–luminosity relation from Equations (2) or (3); ΔV is the velocity width of the emission line, which is taken here as FWHM(Hβ), assuming Doppler broadening (Wandel et al. 1999); and G is the gravitational constant.

The $L/L_{\rm Edd}$ parameter can be computed from the corresponding $M_{\rm BH}$ value following Equation (2) of Shemmer et al. (2010) assuming that $L_{\rm Edd}$ is computed for the case of solar metallicity:

$$L/L_{\rm Edd}\ (L/L_{\rm Edd,\,corr}) = 1.06 f(L)\left[\frac{\nu L_\nu(5100\ \text{Å})}{10^{44}\ \rm erg\ s^{-1}}\right]\left[\frac{M_{\rm BH}\ (M_{\rm BH,\,corr})}{10^6 M_\odot}\right]^{-1}, \quad (5)$$

where $f(L)$ is the luminosity-dependent bolometric correction to νL_ν(5100 Å), derived from Equation (21) of Marconi et al. (2004).

We note that a wide range of bolometric corrections for quasars is available in the literature (e.g., Richards et al. 2006; Nemmen & Brotherton 2010; Runnoe et al. 2012; Netzer 2019). However, in general, the range of these corrections is not large enough to affect the conclusion of our work. For example, Maithil et al. (2022) recently used a constant bolometric correction of $L_{\rm Bol}/\nu L_\nu(5100\ \text{Å}) \sim 9$; the bolometric corrections we derive are in the range of ∼5–6, which results in a relatively small *systematic* offset in the derivation of the $L/L_{\rm Edd}$ parameter.

The uncertainties associated with the corrected $M_{\rm BH}$ and $L/L_{\rm Edd}$ values in this work are estimated to be at least ∼0.3 dex (see Table 2 of Maithil et al. 2022) but could be much larger (∼0.4–0.6 dex) for high $L/L_{\rm Edd}$ objects such as WLQs (see also SL15).

3. Results and Discussion

3.1. Black Hole Masses and Accretion Rates

For the 248 quasars included in this work, we determine the virial Hβ-based $M_{\rm BH,corr}$ and corresponding $L/L_{\rm Edd,corr}$ values from their derived optical properties, following the Fe II-corrected BELR size–luminosity relation of Equation (3), applied to Equations (4) and (5). We also calculate these quasars' $M_{\rm BH}$ and $L/L_{\rm Edd}$ values following the traditional BELR size–luminosity relation of Equation (2) to compare the two methods for estimating black hole masses and accretion rates.

Figure 1 presents the traditional versus corrected $M_{\rm BH}$ and $L/L_{\rm Edd}$ values for the quasars in our sample, following the procedure of Maithil et al. (2022). The Hβ-based $M_{\rm BH,corr}$ values of ordinary quasars show small systematic deviations from the traditional BELR size–luminosity relation estimates (less than a factor of 2 for 222 out of 230 quasars). On the other hand, for a majority of the WLQs, due to the relative weakness in Hβ emission compared to the Fe II emission, $M_{\rm BH,corr}$ values deviate significantly from the traditional relation, by up to 1 order of magnitude. Since $L/L_{\rm Edd}$ is inversely proportional to $M_{\rm BH}$, the $L/L_{\rm Edd,corr}$ values are enhanced by a similar factor. This result is in line with the Maithil et al. (2022) finding of a larger deviation from the one-to-one relation in high-accretion-rate quasars.

3.2. The Anticorrelation between EW(C IV) and L/L_{Edd}

We use our sample to explore the anticorrelation between EW(C IV) and Hβ-based $L/L_{\rm Edd}$ previously studied in SL15 (i.e., the MBE), as well as with $L/L_{\rm Edd,corr}$. Figure 2 shows EW(C IV) plotted against the traditional $L/L_{\rm Edd}$ values (left) and against the Fe II-corrected $L/L_{\rm Edd,corr}$ values (right). The first four rows of Table 3 present the respective Spearman rank correlation coefficients ($r_{\rm S}$) and chance probabilities (p) of the ordinary quasar sample and the complete sample, including WLQs, for the correlation involving EW(C IV). We detect significant anticorrelations between EW(C IV) and $L/L_{\rm Edd}$ both with and without WLQs (i.e., $p \ll 1\%$). However, the anticorrelation for the sample including WLQs is slightly weaker than that without WLQs (both p values are roughly similar, but $r_{\rm S}$ increases slightly). Our result reaffirms findings by SL15, who found WLQs to be outliers in this relation.

With an Fe II correction, the $L/L_{\rm Edd,corr}$ values provide a significantly stronger anticorrelation with EW(C IV) as the $r_{\rm S}$ value decreases from −0.36 (for the $L/L_{\rm Edd}$ case) to −0.48. Furthermore, the inclusion of WLQs no longer spoils the Spearman rank correlation; in fact, the p value remains extremely low ($p = 4.02 \times 10^{-20}$ for the entire sample), and the $r_{\rm S}$ value decreases from −0.48 to −0.54, indicative of a stronger anticorrelation. Nevertheless, the $L/L_{\rm Edd,corr}$ values of most of the WLQs in our sample still appear considerably smaller than a

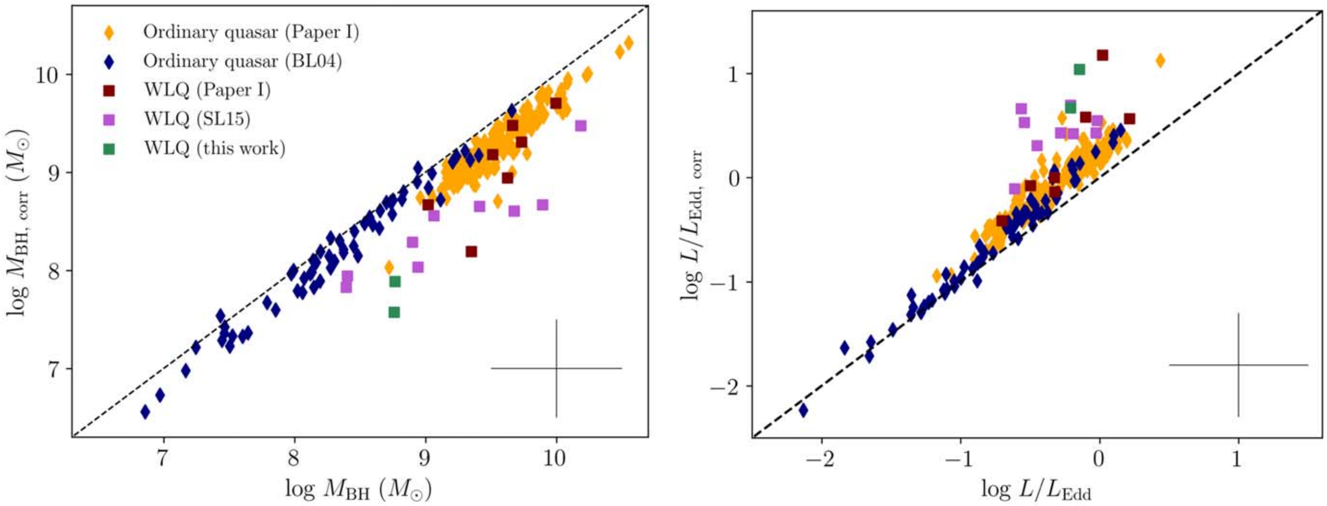

Figure 1. Black hole mass (left panel) and accretion rate (right panel) calculated using the traditional (*x*-axis) and $R_{\rm Fe\ II}$-corrected (*y*-axis) BELR size–luminosity relation for all quasars in our analysis. Diamonds mark ordinary quasars, and squares mark WLQs. The dashed lines represent a one-to-one relation between the two methods. Typical uncertainties of 0.5 dex on the $M_{\rm BH}$ and $L/L_{\rm Edd}$ values are displayed in the bottom right corner of each panel. The traditional relation overestimates $M_{\rm BH}$ in rapidly accreting quasars by up to an order of magnitude. In turn, the traditional relation underestimates $L/L_{\rm Edd}$ by a similar factor. In particular, the $R_{\rm Fe\ II}$-corrected accretion rates are much larger for a considerably larger fraction of sources in the WLQ subset than in the ordinary quasars, due to their larger $R_{\rm Fe\ II}$ values.

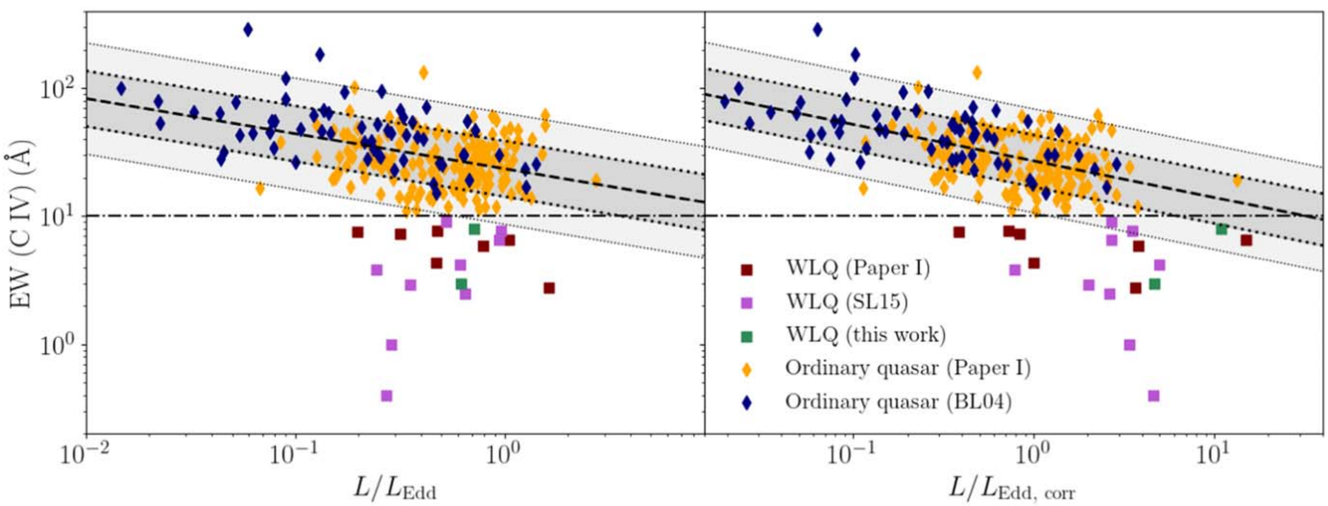

Figure 2. Correlation between EW(C IV) and $L/L_{\rm Edd}$ of ordinary quasars (diamonds) and WLQs from Table 1 (squares). The left panel presents the traditional $L/L_{\rm Edd}$ values, and the right panel displays the Fe II-corrected $L/L_{\rm Edd,corr}$ values. The dotted−dashed lines represent the EW threshold below which objects are defined as WLQs. The correlation for the ordinary quasar sample, obtained by fitting a linear model, is shown as a dashed line. The shaded regions represent the 1σ and 2σ deviations from the fitted correlation. Correcting the traditional $L/L_{\rm Edd}$ values results in a stronger anticorrelation expected by the MBE (see Table 3); however, WLQs' $L/L_{\rm Edd,corr}$ values are still considerably (more than an order of magnitude) overpredicted by the MBE, suggesting that EW(C IV) is not the sole indicator of quasars' accretion rates.

linear model would suggest (see Figure 2). To quantify the deviation of WLQs from the MBE, we fit a simple linear model, without considering the errors, to the log EW(C IV) and log $L/L_{\rm Edd,corr}$ values of the ordinary quasar sample. Our WLQs deviate from the best-fit model by a mean of $\sim 3.4\sigma$, with a range in deviation from 1.08σ to 8.02σ. Such a discrepancy paints WLQs as significant outliers in this correlation.

We also explore whether a bolometric luminosity correction based on the peculiarity of WLQs could account for this discrepancy. Although several methods for correcting bolometric luminosity are available in the literature (e.g., Richards et al. 2006; Nemmen & Brotherton 2010; Runnoe et al. 2012; Netzer 2019), if the Eddington ratios of WLQs were to be reliably predicted by the MBE, these corrections must be up to $\sim 10^5$ times larger than those of Marconi et al. (2004; as in the case of SDSS J1141+0219 with EW(C IV) $= 0.4$ Å). Such a discrepancy is larger than the difference expected by any of the current bolometric correction methods in the literature. These results reveal that EW(C IV) is likely not the sole indicator of accretion rate in all quasars, in agreement with SL15.

3.3. *The C IV ∥ Distance as an Indicator of* L/L_{Edd}

Rivera et al. (2020) used an independent component analysis technique to analyze the spectral properties of the C IV emission line in 133 quasars from the SDSS-RM project (Shen et al. 2015). In particular, they fitted a piecewise polynomial to trace the positions of these sources on the EW(C IV) and the Blueshift

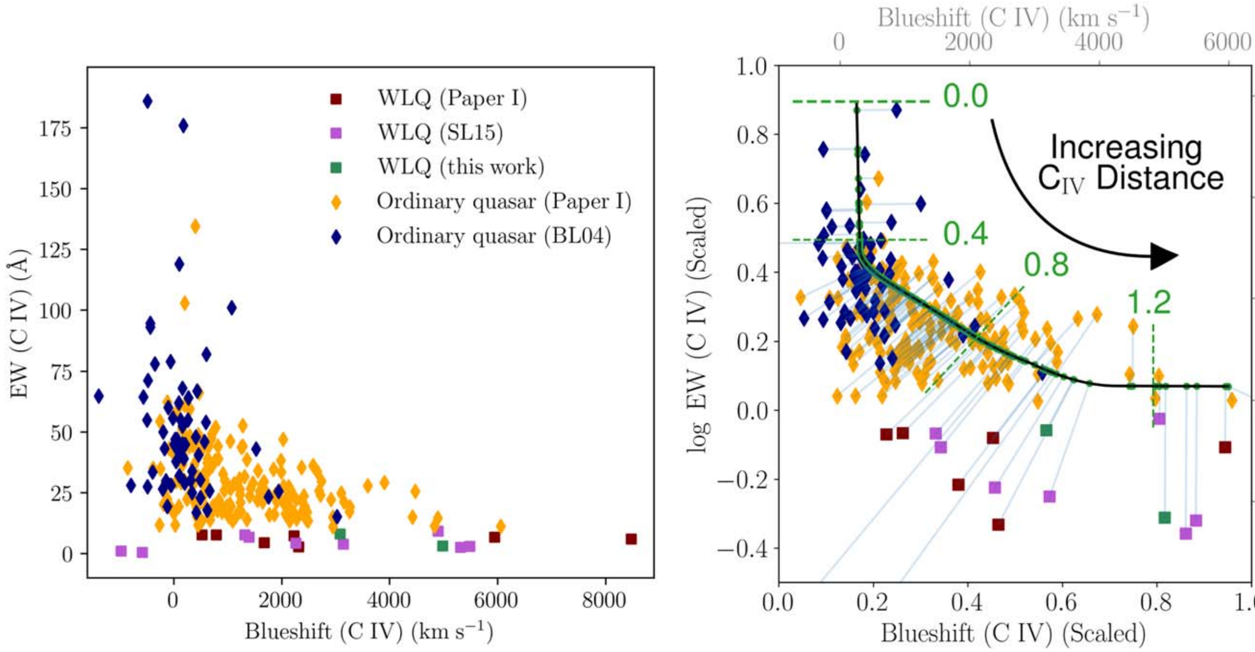

Figure 3. Left panel: distribution of EW(C IV) vs. Blueshift(C IV) for our sample. One quasar from BL04, PG 1202+281, is not shown in the left panel due to its extremely high EW(C IV) =290 Å. Right panel: illustration of the C IV ||Distance parameter. The data are first scaled so that the two axes share the same limit; then, each data point is projected onto the best-fit curve obtained from R22. The C IV ||Distance value of each quasar is defined as its projected position (green point) along the solid black curve. Three of the WLQs, SDSS J114153.33+021924.4, SDSS J123743.07+630144.7, and SDSS J094602.31+274407.0, and one ordinary quasar, PG 1202+281, are not shown in the right panel for clarity, but only their projected positions onto the curve are relevant to our results.

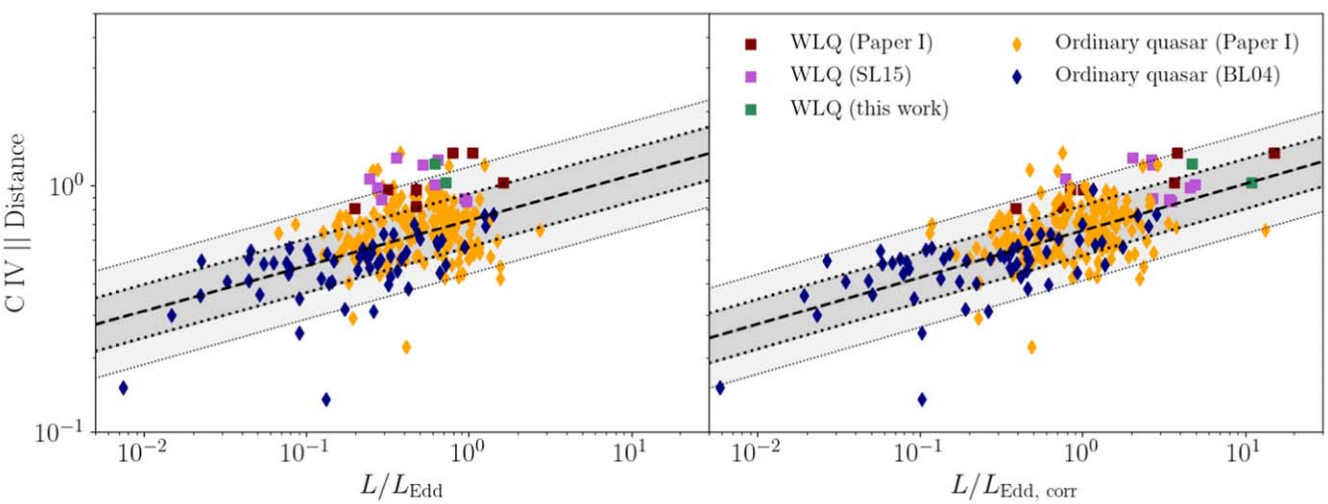

Figure 4. C IV ||Distance vs. $L/L_{\rm Edd}$ of 248 quasars in our sample. In the left panel, the C IV ||Distance values are plotted against the traditional Hβ-based $L/L_{\rm Edd}$ parameter and in the right panel, against the Fe II-corrected Hβ-based $L/L_{\rm Edd,corr}$ parameter. The ordinary quasar PG 1202+281 with $L/L_{\rm Edd,corr}$ =0.06 and C IV ||Distance =0.02 is not plotted for clarity. The correlation for the ordinary quasar sample, obtained by fitting a linear model, is shown as a dashed line. The shaded regions represent the 1σ and 2σ deviations from the fitted correlation. While using the traditional size–luminosity relation to estimate accretion rates already yields a strong correlation, the Fe II-corrected accretion rates show a much stronger correlation with the C IV ||Distance parameter for *all* quasars. Furthermore, this parameter serves as a better predictor for $L/L_{\rm Edd,corr}$ than for $L/L_{\rm Edd}$.

(C IV) plane. The projected position of a quasar along this curve is defined as its "C IV ||Distance." To calculate the value of this C IV ||Distance parameter, we follow the procedure summarized in R22 and detailed in McCaffrey & Richards 2021. In short, we first transform the values of the two axes (EW(C IV) and Blueshift (C IV)) to lie between 0 and 1, using the `MinMaxScaler` function within `scikit-learn` (Pedregosa et al. 2011). Then, the C IV ||Distance values are measured relative to the first point of the best-fit curve, located at EW(C IV) ≈ 316 Å and Blueshift (C IV) ≈ 50 km s^{-1}. This parameter essentially indicates the location along a nonlinear first principal component of the C IV parameter space and encodes information about the physics of the C IV-emitting gas (e.g., Richards et al. 2011, 2021; Giustini & Proga 2019).

The left panel of Figure 3 shows the distribution of EW(C IV) versus Blueshift(C IV) of the 248 quasars in our sample. The right panel of Figure 3 shows the same distribution in scaled space, following the procedure in McCaffrey & Richards (2021), and the piecewise polynomial best-fit curve from Figure 2 of R22. Even though our sources are drawn from

Table 3
Spearman Rank Correlation Coefficients

Correlation	Sample	N	r_S	p
EW(C IV)-$L/L_{\rm Edd}$	Ordinary	230	−0.36	1.39×10^{-8}
EW(C IV)-$L/L_{\rm Edd}$	All	248	−0.35	1.10×10^{-8}
EW(C IV)-$L/L_{\rm Edd,corr}$	Ordinary	230	−0.48	6.82×10^{-15}
EW(C IV)-$L/L_{\rm Edd,corr}$	All	248	−0.54	4.02×10^{-20}
C IV ‖Distance-$L/L_{\rm Edd}$	Ordinary	230	0.37	6.50×10^{-9}
C IV ‖Distance-$L/L_{\rm Edd}$	All	248	0.36	4.17×10^{-9}
C IV ‖Distance-$L/L_{\rm Edd,corr}$	Ordinary	230	0.52	3.16×10^{-17}
C IV ‖Distance-$L/L_{\rm Edd,corr}$	All	248	0.57	1.97×10^{-22}

Note. The last three columns represent the number of sources in each correlation, the Spearman rank correlation coefficient, and the chance probability, respectively.

samples that are different from those of R22, the best-fit curve traces the C IV parameter space of sources across wide ranges of redshifts and luminosities. Since all quasars in our sample are selected photometrically, either in optical (for GNIRS-DQS quasars) or UV (for BL04 quasars) surveys, and were not selected based on their spectroscopic characteristics, there are no known biases associated with their selection, and thus they are expected to trace the C IV parameter space in a similar manner to larger samples of quasars in other studies (e.g., see also Rankine et al. 2020).

While the EW(C IV) parameter, on its own, is not an ideal accretion-rate indicator, the C IV ‖Distance parameter appears to provide a robust indication of the accretion rates for all quasars including WLQs. We plot the C IV ‖Distance versus Hβ-based $L/L_{\rm Edd}$ (left) and $L/L_{\rm Edd,corr}$ (right) for all quasars in our sample in Figure 4. The last four rows of Table 3 provide the Spearman rank correlation coefficients and chance probabilities for the correlations involving the C IV ‖Distance. Both the $L/L_{\rm Edd}$ and $L/L_{\rm Edd,corr}$ are significantly correlated with the C IV ‖Distance parameter (i.e., $p \ll 1\%$).

In the case of C IV ‖Distance versus $L/L_{\rm Edd,corr}$, the correlation coefficient is considerably larger than the correlation involving $L/L_{\rm Edd}$ (0.57 versus 0.36), indicating the importance of the Fe II correction to $M_{\rm BH}$. Furthermore, the inclusion of WLQs in the sample both strengthens the correlation (r_S increases from 0.52 to 0.57, while the p value remains extremely small, $<10^{-16}$) and allows the high-$L/L_{\rm Edd,corr}$ end of the correlation to be more populated. There is also no significant deviation of the WLQs from this correlation, as opposed to their behavior in the MBE (see Figure 2), as well as in the C IV ‖Distance versus traditional $L/L_{\rm Edd}$ (see left panel of Figure 4). To quantify this effect, we fit a linear model to the C IV ‖Distance and $L/L_{\rm Edd}$ ($L/L_{\rm Edd,corr}$) space, taking into account only the ordinary quasars. Then, we calculate the mean scatter of the WLQs from this line. In the case of $L/L_{\rm Edd}$, we find the deviation from the best-fit line to range from 0.62σ to 2.96σ, and the mean deviation to be $\sim 1.8\sigma$. Meanwhile, the deviation in the case of $L/L_{\rm Edd,corr}$ ranges from 0.01σ to 2.18σ, with a mean deviation of $\sim 1.1\sigma$. Thus, using $L/L_{\rm Edd,corr}$ not only results in a stronger correlation with C IV ‖Distance, but C IV ‖Distance also serves as a better predictor for $L/L_{\rm Edd,corr}$ than for $L/L_{\rm Edd}$.

The right panel of Figure 4 shows that WLQs are not a disjoint subset of quasars in the UV-optical space (see also Martínez-Aldama et al. 2018). Our results indicate that WLQs possess relatively high accretion rates due not only to their extremely weak C IV lines but rather to their relatively large values of the C IV ‖Distance parameter. Similarly, we observe quasars with high accretion rates (and large values of C IV ‖Distance) that do not necessarily possess extremely weak C IV lines, some of which have Eddington ratios that are larger than those of several WLQs. Finally, while we are unaware of a large population of quasars that deviate significantly from the correlations of Figure 4, a future examination of, e.g., Hβ-based $L/L_{\rm Edd}$ values of quasars with very large EW(C IV) (e.g., Fu et al. 2022) is warranted to further test our results.

In this work, we show that the C IV and Hβ parameter space provides important diagnostics for quasar physics. In particular, we found that the C IV ‖Distance can serve as a robust predictor of a quasar's accretion rate, especially after a correction based on $R_{\rm Fe\,II}$ is applied. Within the limits of our sample, we also find that WLQs are not a disjoint subset of the type 1 quasar population but instead lie preferentially toward the extreme end of the C IV–Hβ parameter space.

4. Conclusions

We compile a statistically meaningful sample of ordinary quasars and WLQs to study the dependence of quasar accretion rates, corrected for the relative strength of Fe II emission with respect to Hβ, upon source location in the C IV parameter space. Utilizing 18 WLQs, 16 of which are obtained from the literature and two of which are presented in this work, we confirm the findings of Maithil et al. (2022) that the traditional approach to estimating the Eddington ratio for rapidly accreting quasars systematically underestimates this property by up to an order of magnitude compared to Fe II-corrected values of this parameter.

Using the Fe II-corrected values of Hβ-based $L/L_{\rm Edd}$, we investigate the correlation between this parameter and the C IV parameter space. We confirm and strengthen the SL15 results by finding that WLQs spoil the anticorrelation between EW(C IV) and Hβ-based $L/L_{\rm Edd}$ for quasars, whether the latter parameter is estimated using the traditional method or whether a correction based on Fe II emission is employed in the $M_{\rm BH}$ estimate. In keeping with SL15, we conclude that the EW(C IV) cannot be the sole indicator of accretion rate in quasars.

We also investigate the relationships between a recently introduced parameter, the C IV ‖Distance, which is a combination of EW(C IV) and Blueshift(C IV), and the traditional Hβ-based $L/L_{\rm Edd}$ and the Fe II-corrected $L/L_{\rm Edd,corr}$. Such relationships yield strong correlations, especially in the case of Fe II-corrected $L/L_{\rm Edd,corr}$, and can accommodate *all* the quasars in our sample. Our finding suggests that WLQs are not a disjoint subset of sources from the general population of quasars. We find that many WLQs have extremely high accretion rates, which is indicated by their preferentially higher values of the C IV ‖Distance parameter. Similarly, we find several quasars in our sample that possess high Eddington ratios and correspondingly large values of the C IV ‖Distance, which do not have extremely weak C IV lines; some of these sources display Eddington ratios that are larger than those of a subset of our WLQs.

In the context of the C IV parameter space, it will be interesting to investigate whether the extreme X-ray properties of WLQs are the result of extremely large C IV ‖Distance values rather than resulting only from extremely weak C IV lines. Such a test would require X-ray coverage of a large sample of sources with

Hβ + Fe II data across the widest possible C IV parameter space such as the GNIRS-DQS sample of Paper I. It would also be useful to determine whether the weakness of the broad Lyα +N V emission line complex (from which the first high-redshift WLQs were identified) also correlates with C IV ||Distance, which will require rest-frame ultraviolet spectroscopy (Paul et al. 2022). The results of these investigations will shed new light on the connection between the quasar accretion rate and the physics of the inner accretion disk and BELR.

Acknowledgments

This work is supported by National Science Foundation (NSF) grants AST-1815281 (B.M.M., O.S., C.D.), AST-1815645 (M.S.B., A.D.M., J.M.). G.T.R. was supported in part by NASA through a grant (HST-AR-15048.001-A) from the Space Telescope Science Institute, which is operated by the Association of Universities for Research in Astronomy, Incorporated, under NASA contract NAS5-26555. W.N.B. acknowledges support from NSF grant AST-2106990. B.L. acknowledges financial support from the National Natural Science Foundation of China grant 11991053. B.T. acknowledges support from the European Research Council (ERC) under the European Union's Horizon 2020 research and innovation program (grant agreement 950533) and from the Israel Science Foundation (grant 1849/19). We thank an anonymous referee for the insightful comments and suggestions which improved the clarity of this paper. This research has made use of the NASA/IPAC Extragalactic Database (NED), which is operated by the Jet Propulsion Laboratory, California Institute of Technology, under contract with the National Aeronautics and Space Administration.

Software: IRAF (Tody 1986), matplotlib (Hunter 2007), numpy (van der Walt et al. 2011; Harris et al. 2020), pandas (McKinney 2010), scipy (Virtanen et al. 2020), scikit-learn (Pedregosa et al. 2011).

Appendix
NIR Spectroscopy of SDSS J1137+3919 and SDSS J2137−0039

SDSS J113747.64+391941.5 and SDSS J213742.25 −003912.7 (hereafter, SDSS J1137+3919 and SDSS J2137 −0039, respectively) are two WLQs with redshifts suitable for observing the Hβ line in the *H* Band. Observations of these quasars were carried out by the Gemini-North Observatory using GNIRS throughout four observing runs between 2014 March 14 and 2014 August 4, under program GN-2014A-Q-47. The observation log appears in Table A1. For both targets, we used the short blue camera, with spatial resolution $0\farcs15$ pix^{-1} and a $1\farcs0$ slit to achieve a spectral resolution of $R \sim 600$. An *H* filter was applied, producing a spectral range of 1.5–1.8 μm, corresponding to rest-frame ∼4500–5300 Å. Exposure times for each subintegration were 238 and 220 s, and the total integration times were 7140 and 7040 s for SDSS J1137+3919 and SDSS J2137−0039, respectively. These observations were performed using the standard "ABBA" nodding pattern of the targets along the slit in order to obtain primary background subtraction.

The spectra were processed using the standard procedure of the IRAF Gemini package based on the PyRAF Python-based interface. Exposures from the same nodding position were added to boost the signal-to-noise ratio; then, the sum of exposures from two different nodding positions were subtracted to remove background noise. Wavelength calibration was done against an argon lamp in order to assign wavelength values to the observed pixels.

Spectra of telluric standard stars with $T_{\rm eff} \sim 9700$ K were taken immediately before or after the science exposures to remove telluric absorption features in the quasars' observed spectra. These spectra were processed in a similar fashion, followed by a removal of the stars' intrinsic hydrogen absorption lines by fitting a Lorentzian profile to each hydrogen absorption line and interpolating across this feature to connect the continuum on each side of the line. The quasars' spectra were divided by the corrected stellar spectra. The corrected quasar spectra were then multiplied by an artificial blackbody curve with a temperature corresponding to the telluric standard star, which yielded a cleaned, observed-frame quasar spectrum.

Flux calibrations were obtained by taking the Wide-field Infrared Survey Explorer (Wright et al. 2010) *W*1-band (at 3.4 μm) apparent magnitudes, reported by SDSS Data Release 16 (Lyke et al. 2020), and the *W*1 isophotal flux density F_λ(iso) given in Table 1 of Jarrett et al. (2011). Flux densities at 3.4 μm were derived according to

$$F_\lambda(3.4\ \mu{\rm m}) = F_\lambda({\rm iso}) \cdot 10^{-{\rm mag}/2.5}. \quad ({\rm A1})$$

The flux densities at 3.4 μm were extrapolated to flux densities at 1.63 μm, roughly corresponding to $\lambda_{\rm rest} = 5100$ Å, assuming an optical continuum of the form $F_\nu \propto \nu^{-0.5}$ (e.g., Vanden Berk et al. 2001).

We modeled the spectra following the methods of Shemmer et al. (2004) and Shemmer et al. (2010). Our model consists of a linear continuum through the average flux densities of two narrow (∼20 Å) rest-frame bands centered on 4750 and 4975 Å, a broadened Fe II emission template (Boroson & Green 1992), and two Gaussian profiles for the Hβ λ4861 emission line. No [O III] emission lines are detectable in either spectrum, and we placed upper limits on their EWs by fitting a Gaussian feature where the [O III] emission lines should be such that they are indistinguishable from the continuum. The final, calibrated near-infrared spectra of the two WLQs appear in Figure A1.

Table A1
Gemini-North GNIRS *H*-Band Observation Log

Quasar (SDSS J)	z[a]	$z_{\rm sys}$[b]	$\log \nu L_\nu$(5100 Å) (erg s^{-1})	Observation Dates	Exp. Time (s)
113747.64+391941.5	2.420	2.428	45.8	2014 Mar 14, 20	7140
213742.25−003912.7	2.281	2.294	45.8	2014 Jun 29, Aug 04	7040

Notes.
[a] Obtained from visually inspected redshifts (zvis) reported in SDSS Data Release 16 (Lyke et al. 2020).
[b] Systemic redshifts (see the Appendix for details).

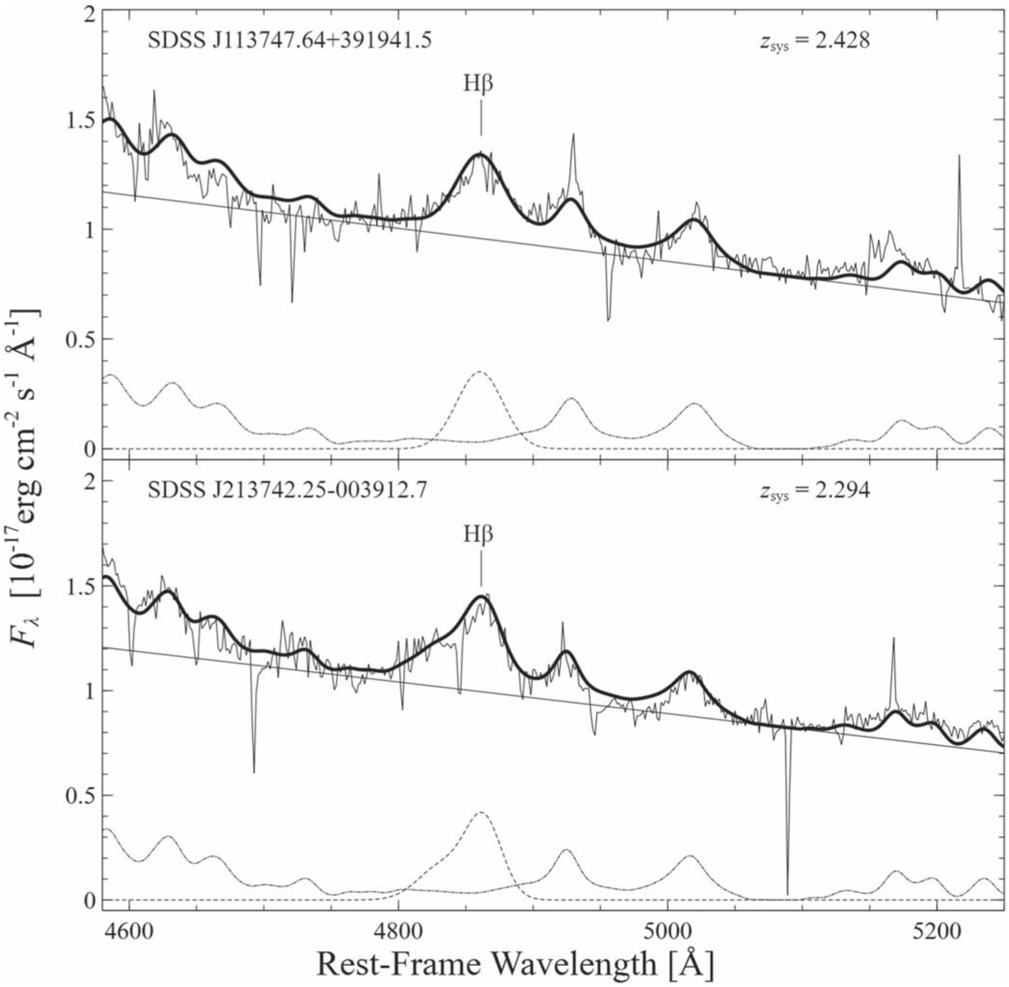

Figure A1. The NIR spectra of SDSS J1137+3919 (top) and SDSS J2137−0039 (bottom). In each panel, the continuous line is the observed spectrum of each quasar. The continuous straight line below the spectrum is the linear continuum fit. The dashed line is the Hβ λ4861 profile modeled with two Gaussians. The dotted−dashed line is the Fe II template from Boroson & Green (1992), which was broadened by 1500 km s^{-1} for SDSS J1137+3919 and 1400 km s^{-1} for J2137−0039. The bold solid line is the entire fitted spectrum.

In both sources we detected weak and relatively narrow Hβ lines as well as strong Fe II features compared to quasars at similar luminosities and redshifts (e.g., see Netzer et al. 2007; Shen 2016). We also determined the systemic redshift (z_{sys}) values from the observed-frame wavelength of the peak (λ_{peak}) of the Hβ emission line, a similar treatment as in Matthews et al. (2021) for sources that lack [O III] emission. The z_{sys} values are larger than the redshifts reported by Lyke et al. (2020) by $\Delta z = 0.008$ in SDSS J1137+3919 and by $\Delta z = 0.013$ in SDSS J2137−0039, corresponding to velocity offsets (blueshifts) of 700 km s^{-1} and 1184 km s^{-1}, respectively, which is consistent with typical velocity offsets between SDSS Pipeline redshifts and z_{sys} values observed in luminous, high-redshift quasars (Dix et al. 2020; Paper I). The rest-frame spectra in Figure A1 have henceforth been corrected by z_{sys}. Rest-frame EWs of Hβ λ4861, Fe II $\lambda\lambda$4434–4684, and the upper limit on the EWs of [O III] λ5007 were calculated for SDSS J1137+3919 to be 16 Å, 53 Å, and $\leqslant$4 Å, and for SDSS J2137−0039 to be 20 Å, 49 Å, and $\leqslant$5 Å, respectively. The flux densities at a rest-frame wavelength of 5100 Å are 7.77×10^{-18} erg cm^{-2} s^{-1} Å^{-1} and 8.18×10^{-18} erg cm^{-2} s^{-1} Å^{-1}, respectively.

ORCID iDs

Trung Ha https://orcid.org/0000-0001-6600-2517
Cooper Dix https://orcid.org/0000-0003-0192-1840
Brandon M. Matthews https://orcid.org/0000-0001-8406-4084
Ohad Shemmer https://orcid.org/0000-0003-4327-1460
Michael S. Brotherton https://orcid.org/0000-0002-1207-0909
Gordon T. Richards https://orcid.org/0000-0002-1061-1804
Jaya Maithil https://orcid.org/0000-0002-4423-4584
Scott F. Anderson https://orcid.org/0000-0002-6404-9562
W. N. Brandt https://orcid.org/0000-0002-0167-2453
Xiaohui Fan https://orcid.org/0000-0003-3310-0131
S. C. Gallagher https://orcid.org/0000-0001-6217-8101
Richard Green https://orcid.org/0000-0003-1245-5232
Paulina Lira https://orcid.org/0000-0003-1523-9164
Bin Luo https://orcid.org/0000-0002-9036-0063
Hagai Netzer https://orcid.org/0000-0002-6766-0260
Richard M. Plotkin https://orcid.org/0000-0002-7092-0326
Jessie C. Runnoe https://orcid.org/0000-0001-8557-2822
Donald P. Schneider https://orcid.org/0000-0001-7240-7449
Michael A. Strauss https://orcid.org/0000-0002-0106-7755

Benny Trakhtenbrot https://orcid.org/0000-0002-3683-7297
Jianfeng Wu https://orcid.org/0000-0001-7349-4695

References

Anderson, S. F., Fan, X., Richards, G. T., et al. 2001, AJ, 122, 503
Baldwin, J. A. 1977, ApJ, 214, 679
Bañados, E., Venemans, B. P., Decarli, R., et al. 2016, ApJS, 227, 11
Baskin, A., & Laor, A. 2004, MNRAS, 350, L31
Baskin, A., & Laor, A. 2005, MNRAS, 356, 1029
Bentz, M. C., Denney, K. D., Grier, C. J., et al. 2013, ApJ, 767, 149
Boroson, T. A., & Green, R. F. 1992, ApJS, 80, 109
Collinge, M. J., Strauss, M. A., Hall, P. B., et al. 2005, AJ, 129, 2542
Diamond-Stanic, A. M., Fan, X., Brandt, W. N., et al. 2009, ApJ, 699, 782
Dix, C., Matthews, B. M., Shemmer, O., et al. 2023, ApJ, 950, 96
Dix, C., Shemmer, O., Brotherton, M. S., et al. 2020, ApJ, 893, 14
Dong, X.-B., Wang, T.-G., Wang, J.-G., et al. 2009, ApJL, 703, L1
Du, P., Hu, C., Lu, K.-X., et al. 2014, ApJ, 782, 45
Du, P., & Wang, J.-M. 2019, ApJ, 886, 42
Du, P., Wang, J.-M., Hu, C., et al. 2016, ApJL, 818, L14
Du, P., Zhang, Z.-X., Wang, K., et al. 2018, ApJ, 856, 6
Fan, X., Strauss, M. A., Gunn, J. E., et al. 1999, ApJL, 526, L57
Fu, S., Brandt, W. N., Zou, F., et al. 2022, ApJ, 934, 97
Giustini, M., & Proga, D. 2019, A&A, 630, A94
Harris, C. R., Millman, K. J., van der Walt, S. J., et al. 2020, Natur, 585, 357
Ho, L. C., & Kim, M. 2014, ApJ, 789, 17
Hryniewicz, K., Czerny, B., Nikołajuk, M., & Kuraszkiewicz, J. 2010, MNRAS, 404, 2028
Hunter, J. D. 2007, CSE, 9, 90
Jarrett, T. H., Cohen, M., Masci, F., et al. 2011, ApJ, 735, 112
Just, D. W., Brandt, W. N., Shemmer, O., et al. 2007, ApJ, 665, 1004
Kaspi, S., Maoz, D., Netzer, H., et al. 2005, ApJ, 629, 61
Kellermann, K. I., Sramek, R., Schmidt, M., Shaffer, D. B., & Green, R. 1989, AJ, 98, 1195
Lane, R. A., Shemmer, O., Diamond-Stanic, A. M., et al. 2011, ApJ, 743, 163
Laor, A. 1998, ApJL, 505, L83
Leighly, K. M., Halpern, J. P., Jenkins, E. B., & Casebeer, D. 2007, ApJS, 173 1
Luo, B., Brandt, W. N., Hall, P. B., et al. 2015, ApJ, 805, 122
Lyke, B. W., Higley, A. N., McLane, J. N., et al. 2020, ApJS, 250, 8
Maithil, J., Brotherton, M. S., Shemmer, O., et al. 2022, MNRAS, 515, 491
Marconi, A., Risaliti, G., Gilli, R., et al. 2004, MNRAS, 351, 169
Marlar, A., Shemmer, O., Anderson, S. F., et al. 2018, ApJ, 865, 92
Martínez-Aldama, M. L., del Olmo, A., Marziani, P., et al. 2018, A&A, 618, A179
Massaro, F., Marchesini, E. J., D'Abrusco, R., et al. 2017, ApJ, 834, 113
Matthews, B. M., Dix, C., Shemmer, O., et al. 2023, ApJ, 950, 95
Matthews, B. M., Shemmer, O., Dix, C., et al. 2021, ApJS, 252, 15
McCaffrey, T. V., & Richards, G. T. C. 2021, CIV Distance, GitHub, doi:10.17918/CIVdistance, https://github.com/RichardsGroup/CIV_Distance
McKinney, W. 2010, in Proc. of the 9th Python in Science Conf., ed. S. van der Walt & J. Millman (Austin, TX: SciPy), 56
Meusinger, H., & Balafkan, N. 2014, A&A, 568, A114
Nemmen, R. S., & Brotherton, M. S. 2010, MNRAS, 408, 1598
Netzer, H. 2019, MNRAS, 488, 5185
Netzer, H., Lira, P., Trakhtenbrot, B., Shemmer, O., & Cury, I. 2007, ApJ, 671, 1256
Netzer, H., Shemmer, O., Maiolino, R., et al. 2004, ApJ, 614, 558
Netzer, H., & Trakhtenbrot, B. 2007, ApJ, 654, 754
Ni, Q., Brandt, W. N., Luo, B., et al. 2018, MNRAS, 480, 5184
Ni, Q., Brandt, W. N., Luo, B., et al. 2022, MNRAS, 511, 5251
Paul, J. D., Plotkin, R. M., Shemmer, O., et al. 2022, ApJ, 929, 78
Pedregosa, F., Varoquaux, G., Gramfort, A., et al. 2011, JMLR, 12, 2825
Plotkin, R. M., Anderson, S. F., Brandt, W. N., et al. 2010, AJ, 139, 390
Plotkin, R. M., Shemmer, O., Trakhtenbrot, B., et al. 2015, ApJ, 805, 123
Rankine, A. L., Hewett, P. C., Banerji, M., & Richards, G. T. 2020, MNRAS, 492, 4553
Richards, G. T., Kruczek, N. E., Gallagher, S. C., et al. 2011, AJ, 141, 167
Richards, G. T., Lacy, M., Storrie-Lombardi, L. J., et al. 2006, ApJS, 166, 470
Richards, G. T., McCaffrey, T. V., Kimball, A., et al. 2021, AJ, 162, 270
Rivera, A. B., Richards, G. T., Gallagher, S. C., et al. 2022, ApJ, 931, 154
Rivera, A. B., Richards, G. T., Hewett, P. C., & Rankine, A. L. 2020, ApJ, 899, 96
Robinson, A. 1994, in ASP Conf. Ser. 69, Reverberation Mapping of the Broad-Line Region in Active Galactic Nuclei, ed. P. M. Gondhalekar, K. Horne, & B. M. Peterson (San Francisco, CA: ASP), 147
Runnoe, J. C., Brotherton, M. S., & Shang, Z. 2012, MNRAS, 422, 478
Shemmer, O., Brandt, W. N., Anderson, S. F., et al. 2009, ApJ, 696, 580
Shemmer, O., Brandt, W. N., Netzer, H., Maiolino, R., & Kaspi, S. 2008, ApJ, 682, 81
Shemmer, O., Brandt, W. N., Schneider, D. P., et al. 2006, ApJ, 644, 86
Shemmer, O., & Lieber, S. 2015, ApJ, 805, 124
Shemmer, O., Netzer, H., Maiolino, R., et al. 2004, ApJ, 614, 547
Shemmer, O., Trakhtenbrot, B., Anderson, S. F., et al. 2010, ApJL, 722, L152
Shen, Y. 2013, BASI, 41, 61
Shen, Y. 2016, ApJ, 817, 55
Shen, Y., Brandt, W. N., Dawson, K. S., et al. 2015, ApJS, 216, 4
Shen, Y., Brandt, W. N., Richards, G. T., et al. 2016, ApJ, 831, 7
Shen, Y., & Ho, L. C. 2014, Natur, 513, 210
Shen, Y., Richards, G. T., Strauss, M. A., et al. 2011, ApJS, 194, 45
Shen, Y., Wu, J., Jiang, L., et al. 2019, ApJ, 873, 35
Spergel, D. N., Bean, R., Doré, O., et al. 2007, ApJS, 170, 377
Timlin, J. D., Brandt, W. N., Ni, Q., et al. 2020, MNRAS, 492, 719
Tody, D. 1986, Proc. SPIE, 627, 733
van der Walt, S., Colbert, S. C., & Varoquaux, G. 2011, CSE, 13, 22
Vanden Berk, D. E., Richards, G. T., Bauer, A., et al. 2001, AJ, 122, 549
Virtanen, P., Gommers, R., Oliphant, T. E., et al. 2020, NatMe, 17, 261
Wandel, A., Peterson, B. M., & Malkan, M. A. 1999, ApJ, 526, 579
Wang, Y., Liu, W., Shang, Z., & Brotherton, M. S. 2022, MNRAS, 515, 5836
Wright, E. L., Eisenhardt, P. R. M., Mainzer, A. K., et al. 2010, AJ, 140, 1868
Wu, J., Brandt, W. N., Anderson, S. F., et al. 2012, ApJ, 747, 10
Wu, J., Brandt, W. N., Hall, P. B., et al. 2011, ApJ, 736, 28
York, D. G., Adelman, J., Anderson, J. E. J., et al. 2000, AJ, 120, 1579
Yu, L.-M., Bian, W.-H., Wang, C., Zhao, B.-X., & Ge, X. 2019, MNRAS, 488, 1519
Yu, L.-M., Bian, W.-H., Zhang, X.-G., et al. 2020a, ApJ, 901, 133
Yu, L.-M., Zhao, B.-X., Bian, W.-H., Wang, C., & Ge, X. 2020b, MNRAS, 491, 5881